

## **Supporting Information**

### **Encapsulating Halide Perovskite Quantum Dots in Metal-Organic Frameworks for Efficient Photocatalytic CO<sub>2</sub> Reduction**

Jingwen Zhang, Wentian Zhou, Junying Chen,\* and Yingwei Li\*

School of Chemistry and Chemical Engineering, State Key Laboratory of Pulp and Paper Engineering, South China University of Technology, Guangzhou 510640, China

\*E-mail: cejychen@scut.edu.cn, liyw@scut.edu.cn

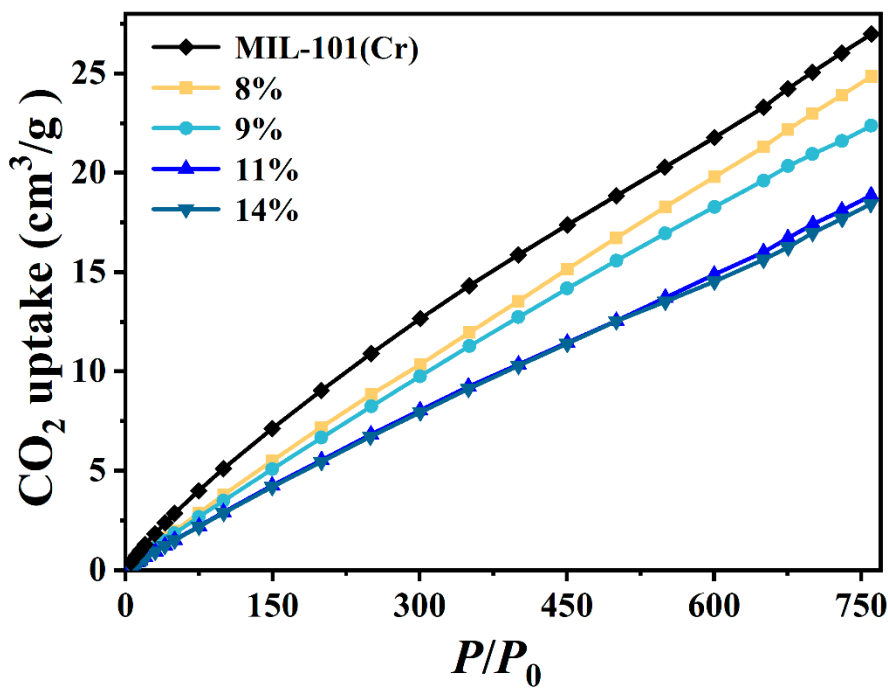


**Figure S1**  $\text{CO}_2$  adsorption isotherms of MIL-101(Cr) and  $x\text{MAPbBr}_3@\text{MIL-101}(\text{Cr})$  at 298 K.

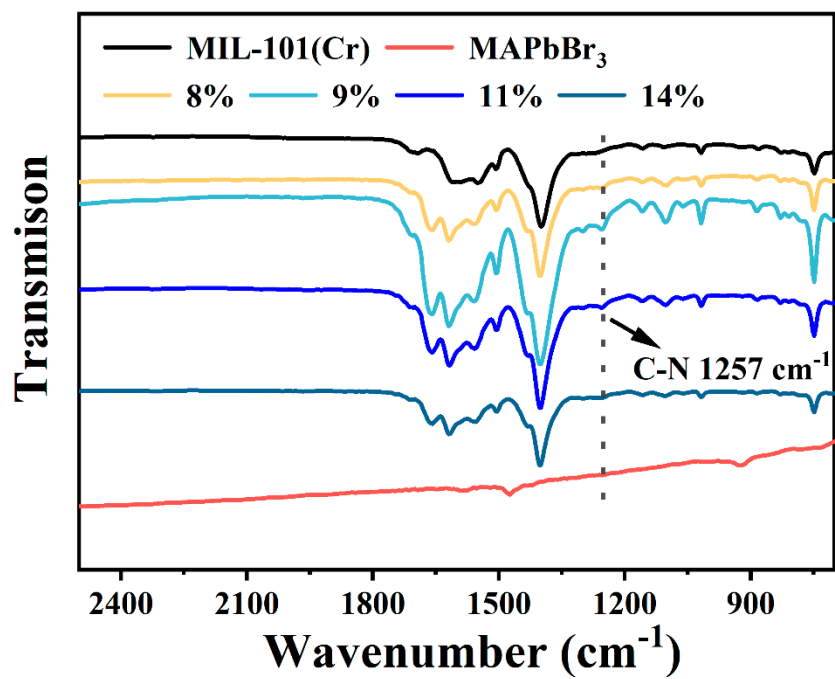


**Figure S2** FTIR spectra of MAPbBr<sub>3</sub>, MIL-101(Cr) and xMAPbBr<sub>3</sub>@MIL-101(Cr).

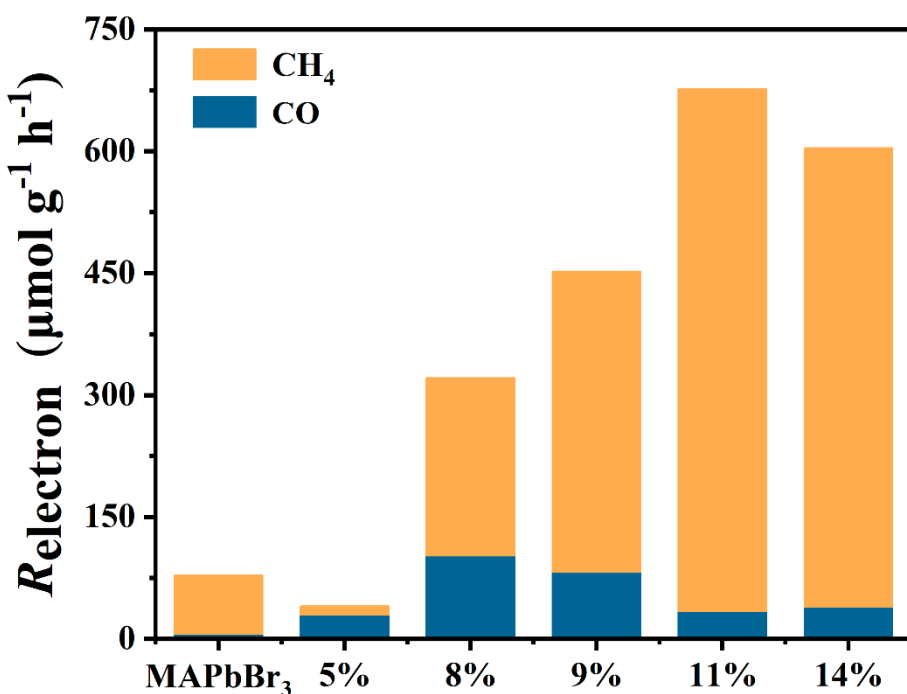


**Figure S3** Electron transfer rate of the  $x\text{MAPbBr}_3@\text{MIL-101}(\text{Cr})$  and  $\text{MAPbBr}_3$  in a 9-h photocatalytic  $\text{CO}_2$  reduction reaction.

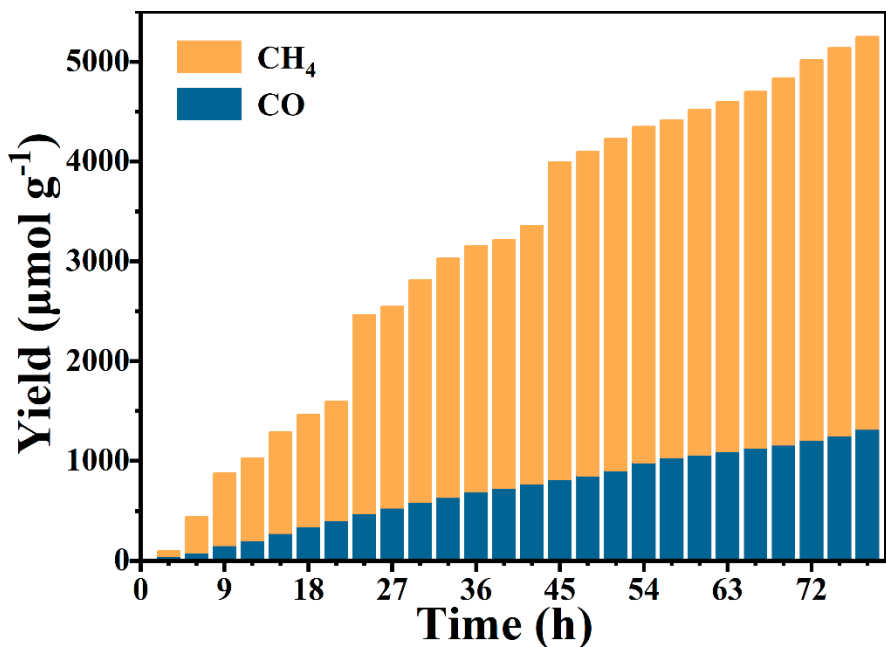


**Figure S4** The yields of  $\text{CH}_4$  and  $\text{CO}$  in a 78-h photocatalytic  $\text{CO}_2$  reduction with 11% $\text{MAPbBr}_3@\text{MIL-101}(\text{Cr})$ .

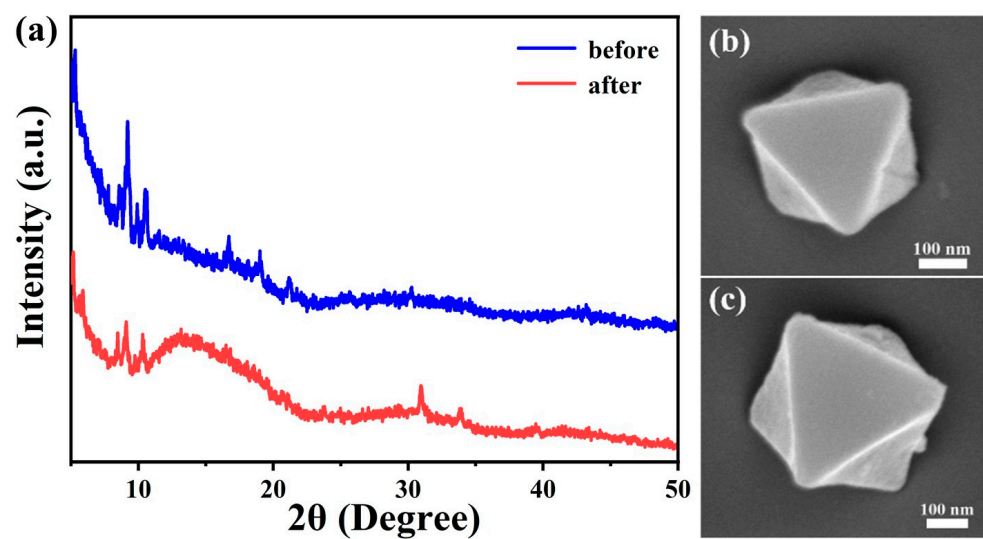


**Figure S5** (a) PXRD patterns and (b, c) SEM images of 11%MAPbBr<sub>3</sub>@MIL-101(Cr) before (b) and after (c) 78 h photocatalytic CO<sub>2</sub> reduction.

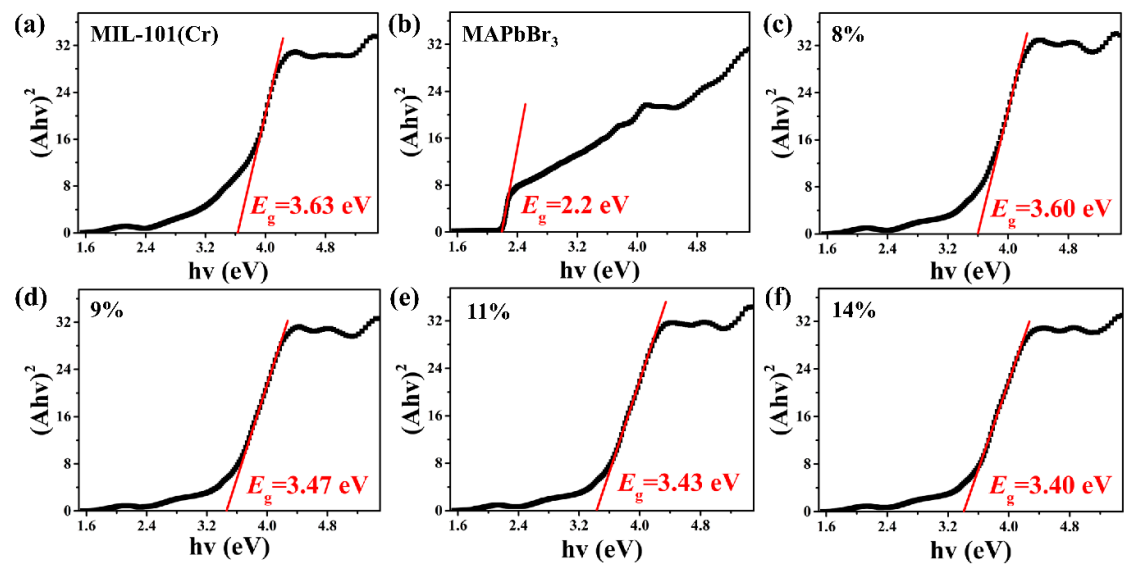


**Figure S6** Tauc plot of MIL-101(Cr) (a), MAPbBr<sub>3</sub> (b) and  $x$ MAPbBr<sub>3</sub>@MIL-101(Cr) (c-f).

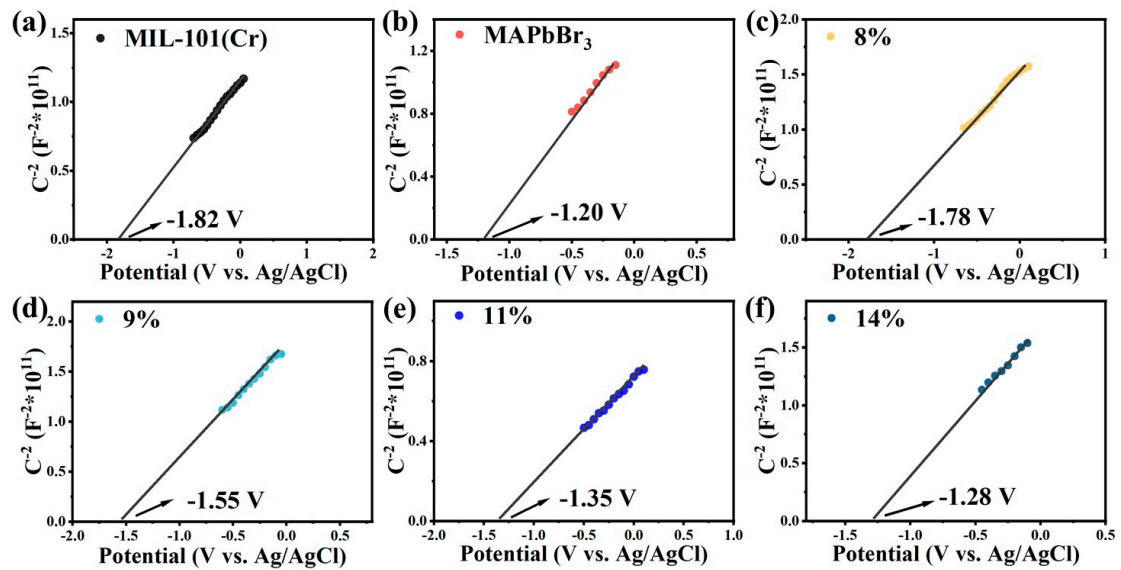


**Figure S7** Mott–Schottky plots (vs. Ag/AgCl) of MIL-101(Cr) (a), MAPbBr<sub>3</sub> (b), and  $x$ MAPbBr<sub>3</sub>@MIL-101(Cr) (c-f).

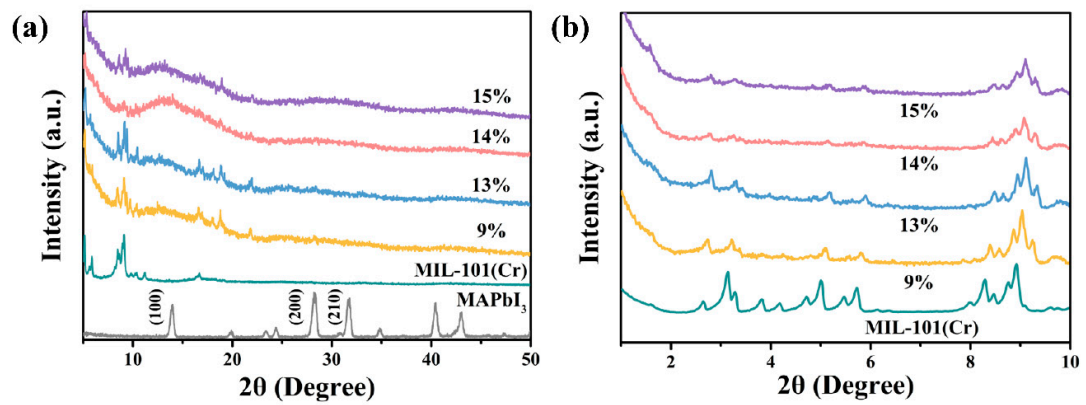


**Figure S8** (a) PXRD patterns and (b) Small-angle XRD patterns of MIL-101(Cr), MAPbI<sub>3</sub>, and  $x$ MAPbBr<sub>3</sub>@MIL-101(Cr) samples.

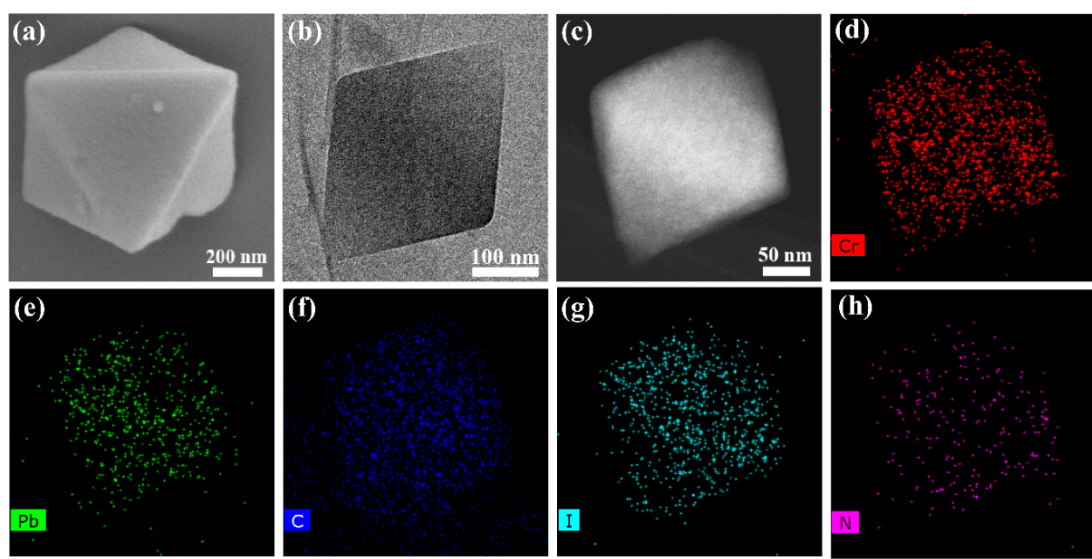


**Figure S9** (a) SEM, (b) TEM, (c) HAADF-STEM images, and (d-h) Elemental mappings of 14%MAPbI<sub>3</sub>@MIL-101(Cr).

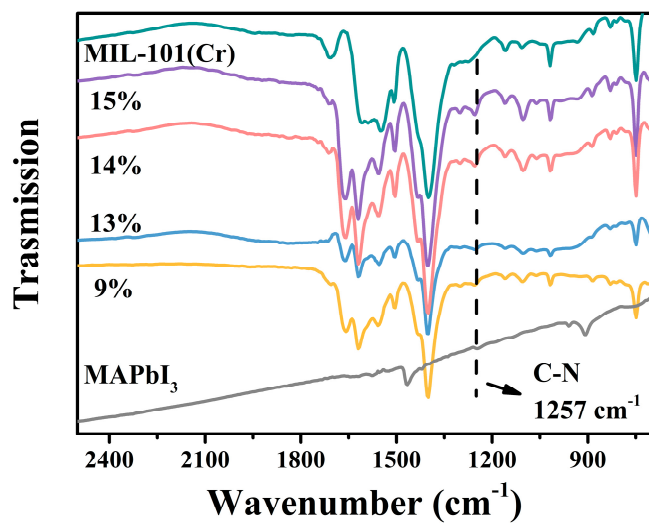


**Figure S10** FTIR spectra of MAPbI<sub>3</sub>, MIL-101(Cr) and  $x$ MAPbI<sub>3</sub>@MIL-101(Cr).

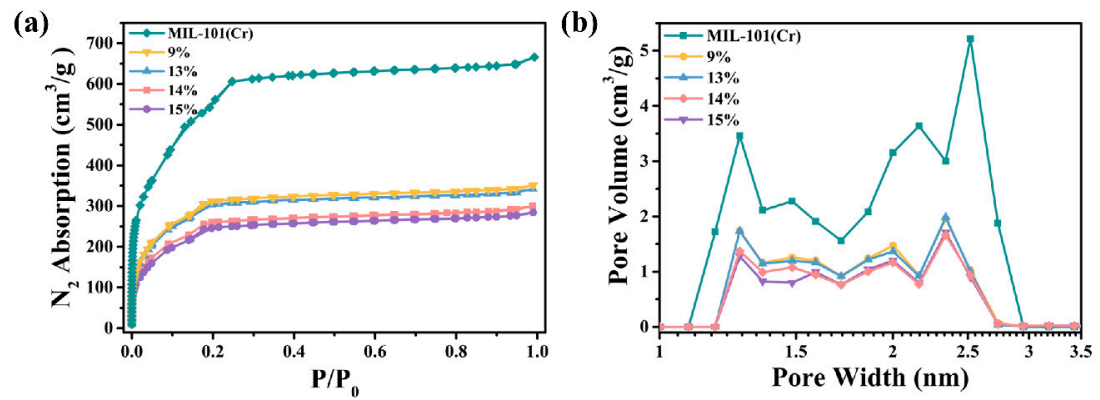


**Figure S11** (a)  $N_2$  sorption isotherms at 77 K and (b) Pore size distribution of MIL-101(Cr) and  $x\text{MAPbI}_3@\text{MIL-101(Cr)}$ .

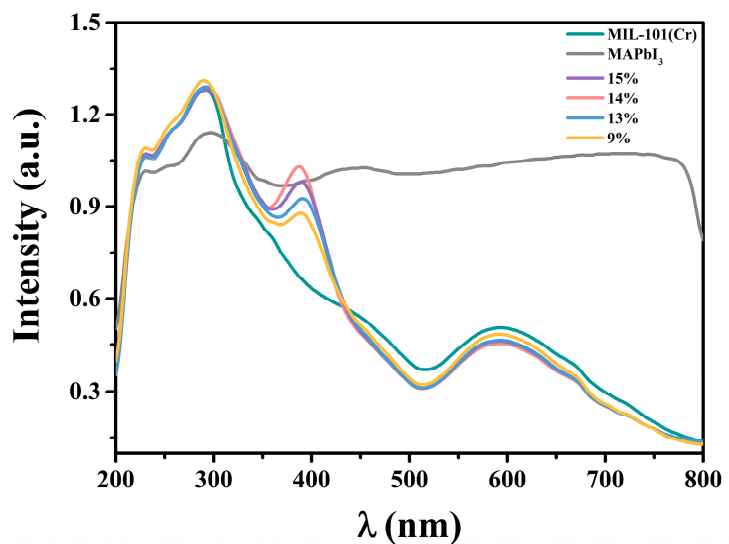


**Figure S12** UV-vis spectra of MIL-101(Cr), MAPbI<sub>3</sub> and xMAPbI<sub>3</sub>@MIL-101(Cr).

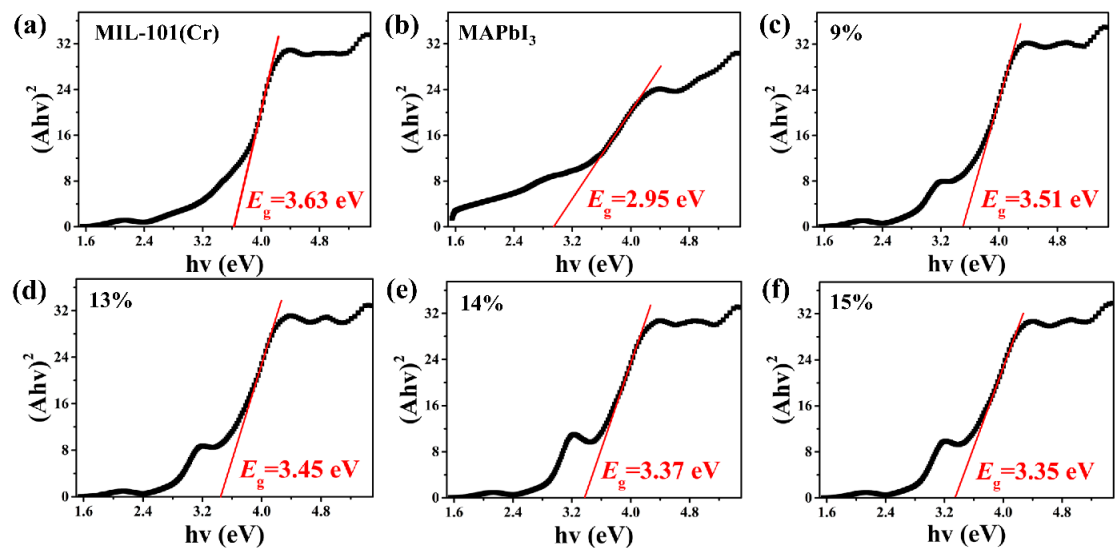


**Figure S13** Tauc plot of MIL-101(Cr) (a), MAPbI<sub>3</sub> (b) and  $x$ MAPbI<sub>3</sub>@MIL-101(Cr) (c-f).

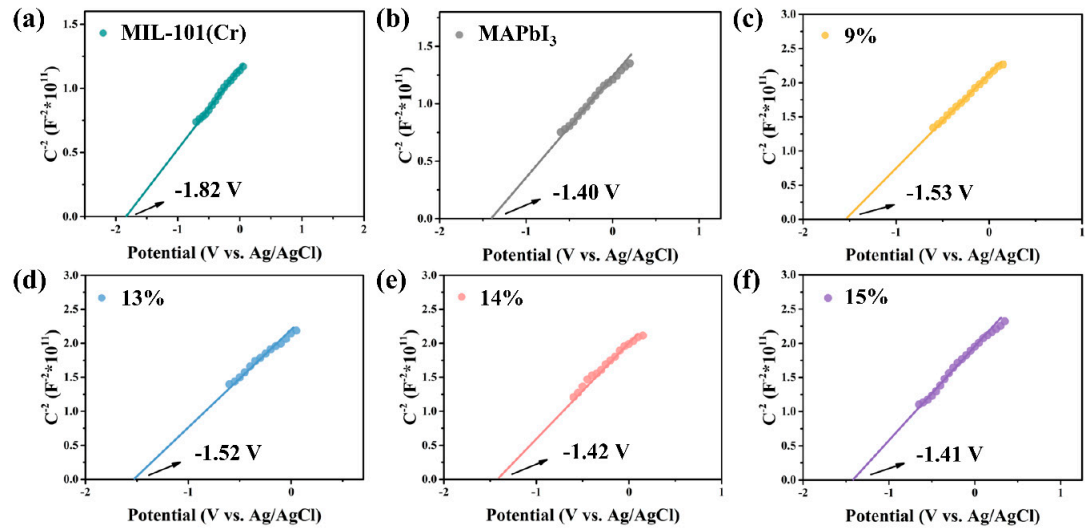


**Figure S14** Mott–Schottky plots (vs. Ag/AgCl) of MIL-101(Cr), MAPbI<sub>3</sub> and  $x$ MAPbI<sub>3</sub>@MIL-101(Cr).

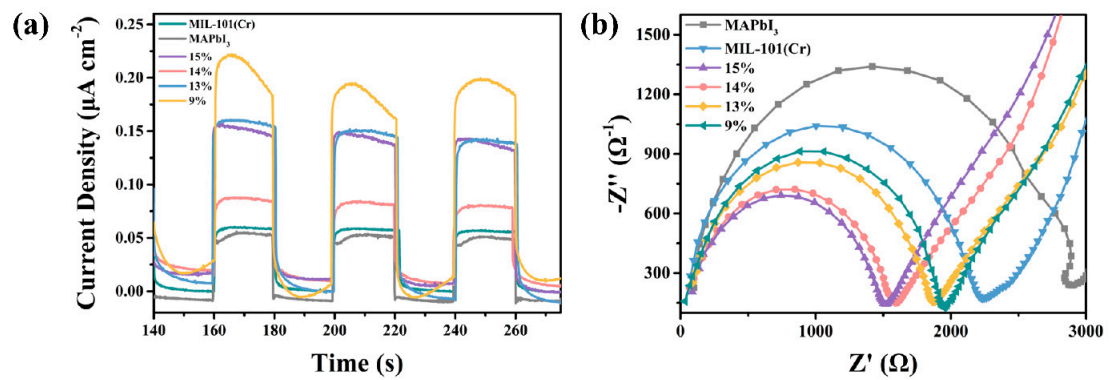


**Figure S15** (a) Photocurrent density curves plotted at 0.2 V (vs. Ag/AgCl) under light and dark, and (b) Electrochemical impedance spectra of MIL-101(Cr), MAPbI<sub>3</sub> and  $x$ MAPbI<sub>3</sub>@MIL-101(Cr).

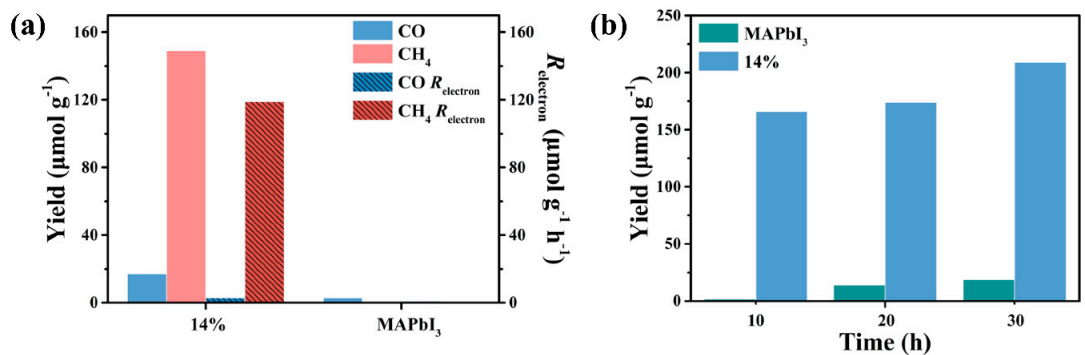


**Figure S16** (a) Yields and  $R_{\text{electron}}$  in a 10-hour reaction, and (b) Stable test of MAPbI<sub>3</sub> and 14%MAPbI<sub>3</sub>@MIL-101(Cr).

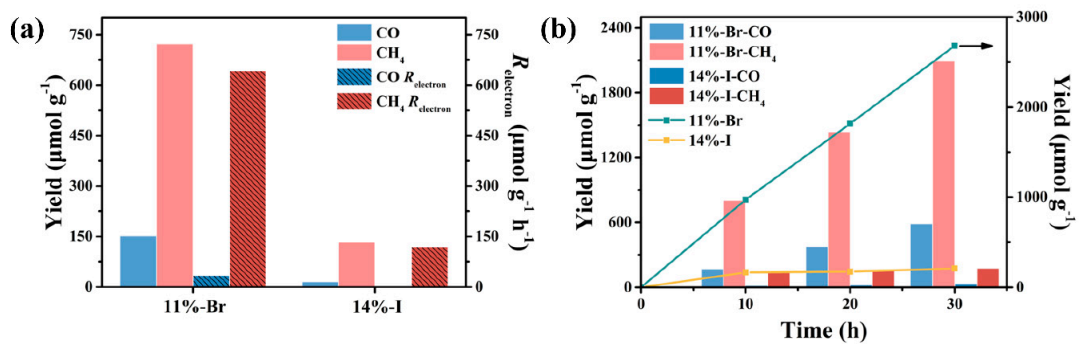


**Figure S17** (a) The comparison of yields and electron consumption rates in a 9-hour reaction, and (b) stability tests in a 30-hour reaction of 11%MAPbBr<sub>3</sub>@MIL-101(Cr) and 14%MAPbI<sub>3</sub>@MIL-101(Cr).

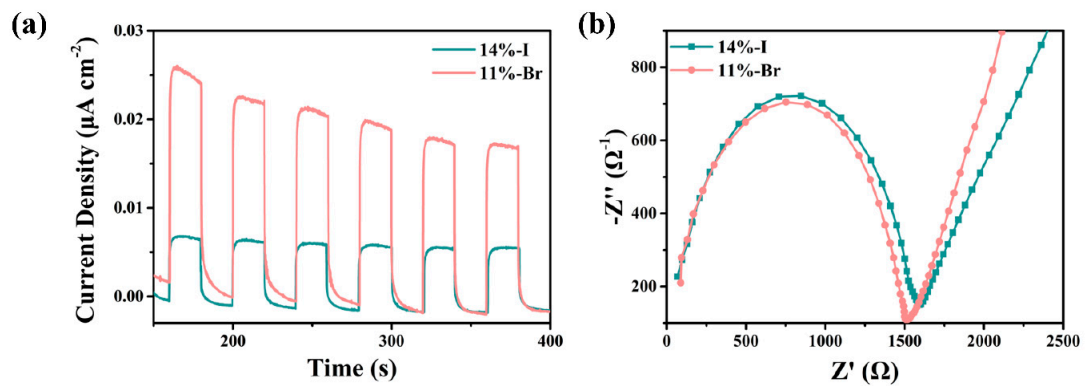


**Figure S18** The comparison of 11MAPbBr<sub>3</sub>@MIL-101(Cr) and 14%MAPbI<sub>3</sub>@MIL-101(Cr) (a) Photocurrent density curves under light and dark. (b) Electrochemical impedance spectra.

**Table S1** Elemental Analysis results of  $x$ MAPbX<sub>3</sub>@MIL-101(Cr)

Sample	Cr (wt%) <sup>a</sup>	Pb (wt%) <sup>a</sup>	MAPbX <sub>3</sub> (wt%) <sup>b</sup>
8%MAPbBr <sub>3</sub> @MIL-101(Cr)	9.52	3.58	8.29
9%MAPbBr <sub>3</sub> @MIL-101(Cr)	8.32	3.90	9.02
11%MAPbBr <sub>3</sub> @MIL-101(Cr)	8.31	4.83	11.17
14%MAPbBr <sub>3</sub> @MIL-101(Cr)	8.54	6.03	13.95
9%MAPbI <sub>3</sub> @MIL-101(Cr)	7.79	2.93	8.77
13%MAPbI <sub>3</sub> @MIL-101(Cr)	8.24	4.36	13.07
14%MAPbI <sub>3</sub> @MIL-101(Cr)	6.89	4.50	13.47
15%MAPbI <sub>3</sub> @MIL-101(Cr)	7.70	4.71	14.09

<sup>a</sup> Measured by ICP-OES. <sup>b</sup> Calculated according to Equation S1

$$wt(MAPBX3)\% = wt_{Pb}\% / \left( \frac{207}{12+6+14+207+80\times 3} \right) \quad (\textbf{Equation S1})$$

**Table S2** Pore volumes of different pores of  $x$ MAPbX<sub>3</sub>@MIL-101(Cr) and MIL-101(Cr)

Sample	Pore volume <sup>a</sup>	Micropore	Mesopore
	(cm <sup>3</sup> /g)	(cm <sup>3</sup> /g)	(cm <sup>3</sup> /g)
MIL-101(Cr)	1.28	0.57	0.71
8%MAPbBr <sub>3</sub> @MIL-101(Cr)	0.72	0.41	0.31
9%MAPbBr <sub>3</sub> @MIL-101(Cr)	0.63	0.41	0.22
11%MAPbBr <sub>3</sub> @MIL-101(Cr)	0.49	0.26	0.23
14%MAPbBr <sub>3</sub> @MIL-101(Cr)	0.47	0.24	0.23
9%MAPbI <sub>3</sub> @MIL-101(Cr)	0.53	0.28	0.71
13%MAPbI <sub>3</sub> @MIL-101(Cr)	0.52	0.28	0.24
14%MAPbI <sub>3</sub> @MIL-101(Cr)	0.45	0.22	0.23
15%MAPbI <sub>3</sub> @MIL-101(Cr)	0.43	0.22	0.21

<sup>a</sup> Total pore volume was determined by using the adsorption branch of the N<sub>2</sub> isotherm at  $P/P_0 = 0.995$ .

**Table S3** Summary of the photocatalytic CO<sub>2</sub> reduction performance over various halide perovskite-based photocatalysts.

Photocatalyst	Products	Light source	R <sub>electron</sub> <sup>a</sup>	Ref.
11%MAPbBr <sub>3</sub> @MIL-101(Cr)	CO, CH <sub>4</sub>	300 W Xe	677	<b>This work</b>
14%MAPbBr <sub>3</sub> @MIL-101(Cr)	CO, CH <sub>4</sub>	300 W Xe	122	<b>This work</b>
CsPbBr <sub>3</sub> /UiO-66(NH <sub>2</sub> )	CO, CH <sub>4</sub>	300 W Xe	18.5	[S1]
CsPbBr <sub>3</sub> /GO	H <sub>2</sub> , CO, CH <sub>4</sub>	100 W	29.8	[S2]
MAPbI <sub>3</sub> @PCN-221(Fe <sub>0.2</sub> )	CO, CH <sub>4</sub>	300 W Xe >400 nm	112	[S3]
CsPbBr <sub>3</sub> /g-C <sub>3</sub> N <sub>4</sub>	CO	300 W Xe >420 nm	148.9	[S4]
CsPbBr <sub>3</sub> @ZIF-8	CO, CH <sub>4</sub>	100 W Xe lamp	15.498	[S5]
CsPbBr <sub>3</sub> @ZIF-67	CO, CH <sub>4</sub>	100 W Xe lamp	29.63	[S5]
Cs <sub>2</sub> SnI <sub>6</sub>	CH <sub>4</sub>	150 mW cm <sup>-2</sup> > 400 nm	16.24	[S6]
Pt-g-C <sub>3</sub> N <sub>4</sub> /NaNbO <sub>3</sub>	CH <sub>4</sub>	300W Xe Lamp > 420 nm	51.2	[S7]
CsPbBr <sub>3</sub> /Au/TiO <sub>2</sub>	CO, CH <sub>4</sub>	AM 1.5 G 100 mW·cm <sup>-2</sup>	44.3	[S9]

<sup>a</sup> The calculation of the total electron consumption rate is based on Equation S2:

$$R_{\text{electron}} = 2R_{\text{CO}} + 8R_{\text{CH}_4} \quad (\textbf{Equation S2})$$

where R<sub>CO</sub> and R<sub>CH<sub>4</sub></sub> represents the generation rate of CO and CH<sub>4</sub>, respectively.

<sup>b</sup> EA = ethyl acetate

**Table S4** TRPL decay parameters of MAPbBr<sub>3</sub>, 11%MAPbBr<sub>3</sub>@MIL-101(Cr) and MIL-101(Cr).

Catalyst	A <sub>1</sub>	τ <sub>1/ns</sub>	A <sub>2</sub>	τ <sub>2/ns</sub>	τ/ns
MAPbBr <sub>3</sub>	68.32	1.72	0.25	8.06	1.82
11%MAPbBr <sub>3</sub> @MIL-101 (Cr)	0.10	25.21	26.98	2.18	3.17
MIL-101 (Cr)	0.16	25.50	32.75	2.03	3.39

$$\tau = \frac{(A_1\tau_1^2 + A_2\tau_2^2)}{(A_1\tau_1 + A_2\tau_2)} \quad (\text{Equation S3})$$

## References

- [1] S. Wan, M. Ou, Q. Zhong, and X. Wang, Perovskite-type CsPbBr<sub>3</sub> quantum dots/UiO-66(NH<sub>2</sub>) nanojunction as efficient visible-light-driven photocatalyst for CO<sub>2</sub> reduction, *Chem. Eng. J.*, **2019**, 358, 1287-1295.
- [2] Y.-F. Xu, M.-Z. Yang, B.-X. Chen, X.-D. Wang, H.-Y. Chen, D.-B. Kuang, and C.-Y. Su, A CsPbBr<sub>3</sub> perovskite quantum dot/graphene oxide composite for photocatalytic CO<sub>2</sub> reduction, *J. Am. Chem. Soc.* **2017**, 139, 5660-5663.
- [3] L.-Y. Wu, Y.-F. Mu, X.-X. Guo, W. Zhang, Z.-M. Zhang, M. Zhang, and T.-B. Lu, Encapsulating Perovskite Quantum Dots in Iron-Based Metal-Organic Frameworks (MOFs) for Efficient Photocatalytic CO<sub>2</sub> Reduction, *Angew. Chem. Int. Ed.* **2019**, 58, 9491–9495.
- [4] M. Ou, W. Tu, S. Yin, W. Xing, S. Wu, H. Wang, S. Wan, Q. Zhong, and R. Xu, Amino-assisted anchoring of CsPbBr<sub>3</sub> perovskite quantum dots on porous g-C<sub>3</sub>N<sub>4</sub> for enhanced photocatalytic CO<sub>2</sub> reduction. *Angew. Chem. Int. Ed.* **2018**, 57, 13570 –13574.
- [5] Z.-C. Kong, J.-F. Liao, Y.-J. Dong, Y.-F. Xu, H.-Y. Chen, D.-B. Kuang, C.-Y. Su, Core@Shell CsPbBr<sub>3</sub>@Zeolitic Imidazolate Framework Nanocomposite for Efficient Photocatalytic CO<sub>2</sub> Reduction, *ACS Energy Lett.* **2018**, 3, 2656–2662.
- [6] X.-D. Wang, Y.-H. Huang, J.-F. Liao, Y. Jiang, L. Zhou, X.-Y. Zhang, H.-Y. Chen, and D.-B. Kuang, In situ construction of a Cs<sub>2</sub>SnI<sub>6</sub> perovskite nanocrystal/SnS<sub>2</sub> nanosheet heterojunction with boosted interfacial charge transfer, *J. Am. Chem. Soc.* **2019**, 141, 13434–13441.
- [7] H. Shi, G. Chen, C. Zhang, and Z. Zou, Polymeric g-C<sub>3</sub>N<sub>4</sub> coupled with NaNbO<sub>3</sub> nanowires toward enhanced photocatalytic reduction of CO<sub>2</sub> into renewable fuel. *ACS Catal.* **2014**, 4, 3637-3643.
- [8] W. Song, K. C. Chong, G. Qi, Y. Xiao, G. Chen, B. Li, Y. Tang, X. Zhang, Y. Yao, Z. Lin, Z. Zou, and B. Liu, Unraveling the transformation from Type-II to Z-scheme in perovskite-based heterostructures for enhanced photocatalytic CO<sub>2</sub> reduction. *J. Am. Chem. Soc.* **2024**, 146, 3303-3314.